Supporting Material for:

A Spatial Model for Integrin Clustering as a Result of Feedback Between Integrin Activation and Integrin Binding

Erik S. Welf[ϕ], Ulhas P. Naik[†], Babatunde A. Ogunnaike[ϕ]

[ϕ]Department of Chemical Engineering, [†]Department of Biological Sciences, University of Delaware

Comparison of simulated integrin clusters with integrin clusters in adherent cells

A subtle difference between the experimental integrin concentration profile shown in Figure 2c and our simulation result shown in Figure 2d is that in the simulation results there is a non-zero concentration of bound integrin far from the cluster nucleation site, whereas in the experimental observation there is no detectable bound integrin outside of the cluster. This may be because the concentration of bound integrin outside of well-defined integrin clusters is too low to be detectable by immunofluorescence, or because physical separation of the cell membrane from the immobilized ECM in regions devoid of clustered integrins precludes visualization by our crosslinking and extraction procedure. In the simulation results, there is no active integrin (or integrin-activating species) far from the nucleation site; the concentration of bound integrin at locations far from the nucleation point is determined by the inactive integrin-ECM binding affinity, and we consider these (low-affinity) bound integrins to be equivalent to the integrins that are not imaged by our experimental procedure as described above. All of the simulation results discussed in this work, exempting those shown in Figure 2d, show only the bound integrin concentration that is greater than the concentration due to basal low-affinity integrin binding, allowing us to focus on clustered integrin and avoid extraneous contributions due to the low concentration of bound, but unclustered integrins present in the simulation results.

Parameter Estimation

Our efforts to determine model parameters from published experimental and modeling studies are summarized in this section. For the subset of parameters whose values could not be determined unambiguously, we employed the following procedure. A series of preliminary model simulations were carried out using a range of values for each of these parameters, allowing us to identify ranges of values for the unknown parameters that are jointly conducive to integrin clustering. The median of this range was then selected as an estimate for each of these parameters.

Because several of the kinetic constants in this model were estimated from data collected in live cells, and since the exact concentration of the different model species at specific locations in a live cell are unknown, all basal intracellular species concentrations are normalized to lie between 0 and 1. This scaling allows the use of apparent reaction rates from live cells, but also introduces an additional parameter, namely the intracellular species concentration, when the apparent intracellular reaction rate is calculated from measurements of chemical reactions outside of a cell. In such cases, an estimate of the reactant concentration near the plasma membrane is used to convert data collected in an acellular environment to apparent intracellular reaction rates.

Integrin-ECM: The rates of integrin-ECM dissociation have been estimated previously from experimental data (1), while the rate of integrin-ECM binding has been estimated from measurements of dissociation rate and dissociation constant (2). Based on these studies, and an estimated integrin concentration of 1000 integrins/μm^2, we select the rate constants for active and inactive integrin binding as 1.5 s^{-1} and 0.34 s^{-1}, respectively (3). The rate constants for active and inactive integrin unbinding have been determined experimentally as 0.1 s^{-1}, and 3.4 s^{-1}, respectively (1).

Talin-integrin: Although the inactive, auto-inhibited form of talin prevents interactions between the talin F3 domain and integrin tails, the active form adopts an unclasped structure that allows the talin F3 domain to bind integrin cytoplasmic tails with high affinity (4). Therefore, we use the binding constants obtained for the talin F3 domain to represent the active form of talin and assume that inactive talin does not interact with integrin tails (5). Because the studies used to obtain the binding and unbinding rates for this interaction were performed *in vitro*, we used an estimated concentration of talin *at the plasma membrane* (100 μM) to obtain the effective binding rate of active talin to free integrin at the membrane; thus our estimate for k_{1f} is 3.3 s^{-1}. Our estimate for k_{1r}, 0.0042 s^{-1}, is taken directly from Calderwood et al. (5). We estimated the rate constants for binding and unbinding of active talin to bound integrin based on the required steady state relationships between rate constants, and from the established values for k_{1f}, k_{1r}, k_{2f}, k_{2r}, k_{3f}, and k_{3r}. Specifically, at steady state

$$[IET] = \frac{k_{1f}}{k_{1r}} \frac{k_{2f}}{k_{2r}} = \frac{k_{3f}}{k_{3r}} \frac{k_{4f}}{k_{4r}} \quad (1)$$

and as a result, $k_{4f}/k_{4r} = 1.78 \times 10^5$. Assuming that the off-rate for talin dissociating from bound integrin is the same under all conditions, we determine that $k_{4f} = 495\ s^{-1}$. This relatively fast reaction rate may be due to a conformational change effected when inactive integrins bind ECM, thus increasing the accessibility of the talin binding site on the integrin tail.

PIPKIγ: Because PIPKIγ has been shown to target focal adhesions via numerous focal adhesion proteins, but there have been no reports quantifying the rate of binding of PIPKIγ to a specific docking site, we estimated the rate of PIPKIγ reaction with bound integrins via talin by determining the values of k_{5f} that result in integrin clustering. It was determined that low (<1 s^{-1}) values of k_{5f} result in very dispersed regions of bound integrin, whereas high (>10 s^{-1}) values result in the higher local concentrations of bound integrin that are indicative of integrin clusters. Therefore, the baseline value for k_{5f} was set to 100 s^{-1}. For the purposes of this study, we are concerned with initial formation of integrin clusters, which is known to occur in a thin region at the front of the lamellipodium (6). These clusters are stable until they reach the lamellipodium-lamella boundary, at which point they either turn over (disperse) or mature (grow) into stable adhesions. Since we are interested in the mechanisms of initial integrin cluster formation, we assume that the biochemical conditions present in the lamellipodium stabilize integrins bound to talin and PIPKIγ. Consequently, we assume that reaction 5 is irreversible and thus set the constant k_{5r} to zero in all of our simulations except as noted in the section titled *Integrin clustering dynamics and cluster turnover* in the main text of this paper.

PIP phosphorylation and degradation: The rate constants for stimulated PIP phosphorylation by PIPKIγ (k_6) and PIP2 dephosphorylation (k_7) were initially chosen to be 0.92 s^{-1} and 2.4 s^{-1}, respectively, as previously determined (7). However, the value $k_6 = 0.92\ s^{-1}$ produced large and dispersed integrin clusters; to produce a smaller denser cluster, the value was reduced to 0.2 s^{-1}. This value corresponds to a rate of PIP phosphorylation slightly slower than the rate of stimulated PIP phosphorylation in neuroblastoma cells, making it appropriate for conditions when PIP phosphorylation is slightly slower than under the “stimulated” conditions represented in the work by Xu et al.

Talin activation by PIP2: Previous experimental studies have indicated that the association constant for talin binding PIP2 is relatively large (3 μM^{-1}) (8), and also that the kinetics of PIP2 association with talin are rapid in spreading cells (9); therefore, we estimate the rate constants for k_{8f} and k_{8r} as 50 s^{-1} and 0.01 s^{-1}, respectively.

Diffusion coefficients: Any species not bound to ECM is considered mobile, whereas any species bound directly or indirectly to ECM is considered immobile. We consider diffusion and reaction of proteins only in a very small segment (<1μm) of the cytosol adjacent to the cell membrane; we do not explicitly model exchange of cytosolic proteins between the membrane-associated fraction and the bulk cytosolic compartment. The diffusivities of cytosolic species within the membrane-associated compartment are set to an arbitrarily high value.

Experimental measurements of adhesion receptor diffusion indicate that free adhesion receptor diffusivity ranges from 0.01 to 20 $\mu m^2/s$ (10,11) from which we estimate D_I to be 0.01 $\mu m^2/s$. Although talin and PIPKIγ reside in the cytosol and are capable of diffusing in three dimensions, we consider only a thin portion of the cytosol that is in contact with a membrane segment a few microns in length, and therefore neglect any exchange of cytosolic species between the membrane-proximal space and the bulk cytosol. The diffusivity of free cytosolic proteins of approximately 200 kDa in size is known to be in the range 1-10 $\mu m^2/s$ (12). Since PIPKIγ is approximately 90 kDa in size, we estimated $D_{PIPKI\gamma}$ to be 1 $\mu m^2/s$. Full length talin is approximately 250 kDa in size and D_T was estimated to be 1 $\mu m^2/s$ for inactive (cytosolic) talin; the D_{T^*} for active (membrane-associated) talin was set at 0.01 $\mu m^2/s$,. Several studies have reported the diffusivity of free phospholipids to be in the range 0.5-2 $\mu m^2/s$ (13–15); as such, initially we estimated D_{PIP} and D_{PIP2} to be 1 $\mu m^2/s$. However, lower diffusivity was required for integrin clustering; the baseline D_{PIP} was therefore reduced to 0.01 $\mu m^2/s$. As with talin, the diffusivity of phospholipids has been shown to depend on their association with cytoskeletal components (16) or membrane microdomains (15), and it has been shown that lipid diffusivity is impaired at the leading edge of a migrating cell (17). It is therefore reasonable to assume that phospholipids in a region of the cell where integrin clustering is occurring would be susceptible to impaired diffusivity, compared to the free phospholipids. The observation that integrin clustering by the proposed mechanism requires such a low diffusivity of PIP2 suggests that reduced PIP2 mobility within the aforementioned spatial domains may help facilitate clustering therein, and prevent clustering in other regions of the cell. Assuming that both types of phospholipids exhibit equivalent diffusivities in the region considered in this work, D_{PIP2} was set equal to D_{PIP}.

Initial species concentrations: All baseline initial species concentrations were set to zero at t=0, except for $[I]_o^*$, $[E]_o^*$, $[T]_o^*$, $[K]_o^*$, $[PIP]_o^*$, and a nucleation species, all of which must have nonzero initial value for integrin clustering to occur. The baseline values for all intracellular species concentrations are normalized to fall between 0 and 1. Because it was desired to simulate conditions where ECM is in abundance and intracellular conditions limit integrin clustering, $[E]_o^*$ was set to 2, and $[I]_o^*$ was set to 0.25. Inactive talin is a cytosolic protein and to model the effect of free exchange with the active, membrane-associated form we set $[T]_o^*$ to 1. It was determined that lower values (<1) of PIP and PIPKIγ were required to prevent integrin clusters from spreading across the entire simulation space; therefore $[P]_o^*$ and $[K]_o^*$ were set to 0.2 and 0.1, respectively.

Experimental Methods

To study integrin spatial distribution, we utilized a technique that labels bound integrins via their cytoplasmic domain (18,19). Chinese Hamster Ovary (CHO) cells stably expressing the integrin αIIbβ3 were grown in Dulbecco's Modified Eagle Medium (DMEM) containing 10% Fetal Bovine Serum (FBS) and 300 μg/ml of G418, and were serum starved with DMEM containing 0.5% Bovine Serum Albumin (BSA) 12 hours prior to treatment. Glass coverslips were prepared for cell adhesion assay by coating with various concentrations of fibrinogen (Fg) in Phosphate Buffered Saline (PBS) for 12 hours at 4^oC immediately prior to cell adhesion. Cells were released from culture dishes by versene, then washed once with 0.5% BSA in DMEM. Cells were then plated onto the coverslips and incubated at 37^oC. After cells were allowed to adhere for two hours, coverslips were washed once with PBS and then extracellular proteins were crosslinked with 0.4mM Bissulfosuccinimidyl suberate (BS3) for 15 minutes. The crosslinking reaction was then quenched with 20 mM Tris-HCl for two minutes and washed twice with PBS. Uncrosslinked proteins were then extracted with 0.5% NP-40 in PBS for ten minutes, and then coverslips were washed twice with PBS. The remaining proteins were then fixed using 4% paraformaldehyde for ten minutes, and washed twice with PBS. Coverslips containing cell remnants were then blocked overnight at 4^oC using 3% BSA in PBS, then incubated with primary antibody, anti-integrin β3 (C-20) goat IgG from Santa Cruz, for one hour at 37^oC. Coverslips were then washed three times with PBS and incubated with secondary antibody (Alexa Fluor 568 Donkey anti-goat IgG from Invitrogen) along with fluorescein-labeled phalloidin for one hour at 37^oC, then washed an additional three times before mounting and imaging. Images were collected using a Zeiss LSM confocal microscope with Plan-Apochromate 63x Oil objective (1.4 NA) and a pinhole size set to 1 Airy unit.

Individual integrin cluster intensity profiles were extracted from the integrin intensity image matrix by identifying a single row or column of the intensity matrix that bisected an individual integrin cluster at the approximate center, and plotting the fluorescence intensity vs the coordinates of the pixels along the row or column. All image processing and analysis steps were performed on the Matlab platform (Mathworks, Natick MA).

Computational Methods

All simulations were performed on the Matlab platform using the *matmol* algorithm (20). Equations 9-18 were solved on a spatial grid $x \in [0, 1]$ having 51 mesh nodes, time $t \in [0, 300]$, and employing no flux boundary conditions.

References

1. Vitte J, Benoliel A-M, Eymeric P, Bongrand P, Pierres A. Beta-1 integrin-mediated adhesion may be initiated by multiple incomplete bonds, thus accounting for the functional importance of receptor clustering. Biophys. J. 2004 Jun;86(6):4059–74.

2. Iber D, Campbell ID. Integrin activation--the importance of a positive feedback. Bull. Math. Biol. 2006 May;68(4):945–56.

3. Ward MD, Hammer DA. A theoretical analysis for the effect of focal contact formation on cell-substrate attachment strength. Biophys. J. 1993 Mar;64(3):936–59.

4. Goksoy E, Ma Y-Q, Wang X, Kong X, Perera D, Plow EF, et al. Structural basis for the autoinhibition of talin in regulating integrin activation. Mol. Cell. 2008 Jul 11;31(1):124–33.

5. Calderwood DA, Yan B, de Pereda JM, Alvarez BG, Fujioka Y, Liddington RC, et al. The phosphotyrosine binding-like domain of talin activates integrins. J. Biol. Chem. 2002 Jun 14;277(24):21749–58.

6. Choi CK, Vicente-Manzanares M, Zareno J, Whitmore LA, Mogilner A, Horwitz AR. Actin and α-actinin orchestrate the assembly and maturation of nascent adhesions in a myosin II motor-independent manner. Nat Cell Biol. 2008 Sep;10(9):1039–50.

7. Xu C, Watras J, Loew LM. Kinetic analysis of receptor-activated phosphoinositide turnover. J. Cell Biol. 2003 May 26;161(4):779–91.

8. Goldmann WH, Senger R, Kaufmann S, Isenberg G. Determination of the affinity of talin and vinculin to charged lipid vesicles: a light scatter study. FEBS Lett. 1995 Jul 24;368(3):516–8.

9. Martel V, Racaud-Sultan C, Dupe S, Marie C, Paulhe F, Galmiche A, et al. Conformation, localization, and integrin binding of talin depend on its interaction with phosphoinositides. J. Biol. Chem. 2001 Jun 15;276(24):21217–27.

10. Chan PY, Lawrence MB, Dustin ML, Ferguson LM, Golan DE, Springer TA. Influence of receptor lateral mobility on adhesion strengthening between membranes containing LFA-3 and CD2. J. Cell Biol. 1991 Oct;115(1):245–55.

11. Hirata H, Ohki K, Miyata H. Mobility of integrin alpha5beta1 measured on the isolated ventral membranes of human skin fibroblasts. Biochim. Biophys. Acta. 2005 May 25;1723(1-3):100–5.

12. Arrio-Dupont M, Foucault G, Vacher M, Devaux PF, Cribier S. Translational diffusion of globular proteins in the cytoplasm of cultured muscle cells. Biophys. J. 2000 Feb;78(2):901–7.

13. Haugh JM, Codazzi F, Teruel M, Meyer T. Spatial sensing in fibroblasts mediated by 3’ phosphoinositides. J. Cell Biol. 2000 Dec 11;151(6):1269–80.

14. van Rheenen J, Jalink K. Agonist-induced PIP(2) hydrolysis inhibits cortical actin dynamics: regulation at a global but not at a micrometer scale. Mol. Biol. Cell. 2002 Sep;13(9):3257–67.

15. Yechiel E, Edidin M. Micrometer-scale domains in fibroblast plasma membranes. J. Cell Biol. 1987 Aug;105(2):755–60.

16. Cho H, Kim YA, Yoon J-Y, Lee D, Kim JH, Lee SH, et al. Low mobility of phosphatidylinositol 4,5-bisphosphate underlies receptor specificity of Gq-mediated ion channel regulation in atrial myocytes. Proc. Natl. Acad. Sci. U.S.A. 2005 Oct 18;102(42):15241–6.

17. Weisswange I, Bretschneider T, Anderson KI. The leading edge is a lipid diffusion barrier. J. Cell. Sci. 2005 Oct 1;118(Pt 19):4375–80.

18. Keselowsky BG, García AJ. Quantitative methods for analysis of integrin binding and focal adhesion formation on biomaterial surfaces. Biomaterials. 2005 Feb;26(4):413–8.

19. Welf ES, Ogunnaike BA, Naik UP. Quantitative statistical description of integrin clusters in adherent cells. IET Syst. Biol. 2009;3(5):307.

20. Wouwer A, Saucez P, Schiesser W, Thompson S. A MATLAB implementation of upwind finite differences and adaptive grids in the method of lines. Journal of computational and applied mathematics. 2005 Nov 15;183(2):245–58.

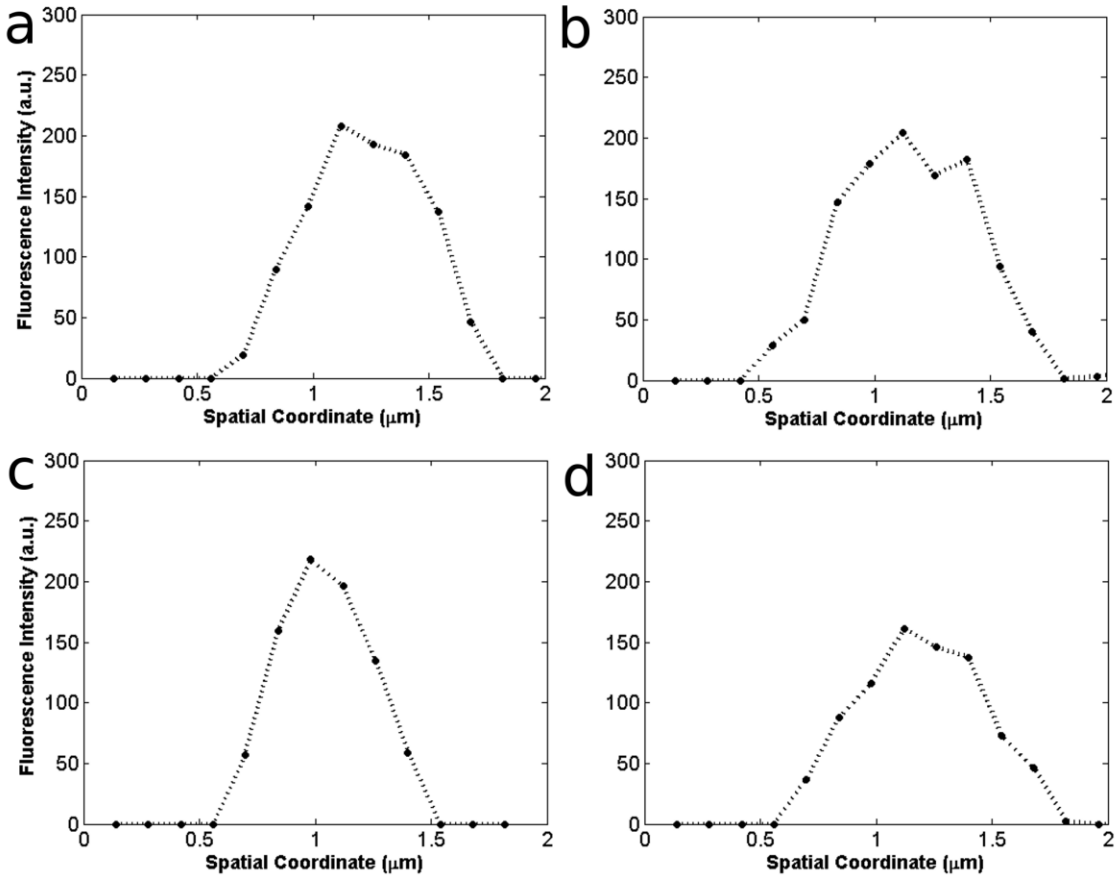

Figure S1. Additional examples of measured nascent integrin cluster profiles.